Applied Surface Science 256 (2010) 4402–4407

Contents lists available at ScienceDirect

Applied Surface Science

journal homepage: www.elsevier.com/locate/apsusc

Atomistic modeling of β-Sn surface energies and adatom diffusivity

Michael S. Sellers [a,*], Andrew J. Schultz [a], Cemal Basaran [b], David A. Kofke [a]

[a] Department of Chemical and Biological Engineering, University at Buffalo, The State University of New York, Buffalo, NY 14260, USA
[b] Electronics Packaging Laboratory, Department of Civil, Structural and Environmental Engineering, University at Buffalo, The State University of New York, Buffalo, NY 14260, USA

ARTICLE INFO

Article history:
Received 2 September 2009
Received in revised form 11 February 2010
Accepted 12 February 2010
Available online 19 February 2010

Keywords:
Tin surface diffusion
Tin surface energy
Electromigration

ABSTRACT

Energies for low number Miller index surfaces of β-Sn (b.c.t. structure) were computed and the (1 0 0) plane was found to have the lowest un-relaxed energy of 0.0497 eV/Å^2. We then used the Dimer method to find mechanisms and corresponding activation energies, E_A, for a Sn adatom moving on a β-Sn (1 0 0) surface. After extensive dimer searches and comparison to long molecular dynamics simulations, we conclude that two simple hopping mechanisms dominate transitions on this surface. For each, we determined hopping rates of the adatom using transition state theory and computed its tracer diffusivity. A hop of the adatom in the lattice *c*-direction gives $D_{300\,K} = 1.893 \times 10^{-06}$ cm^2/s ($E_A = 0.1493$ eV), while in the lattice *a*-direction $D_{300\,K} = 3.994 \times 10^{-06}$ cm^2/s ($E_A = 0.1138$ eV). When compared to studies on the existence of low energy multi-atom adatom diffusion on Cu and Al (1 0 0), we assert that β-Sn's successive (2 0 0) plane layering in the [1 0 0] direction provides for significantly lower activation energies and may contribute to the inability to locate any concerted atomic motion mechanisms.

1. Introduction

Most of the thermodynamic formulations describing failure due to electromigration and/or thermomigration employ atomistic transport quantities determined experimentally. For example, Kirchhiem's model [1,2], extended by Basaran et al. [3,4] describes the temporal vacancy concentration in a Sn solder joint based on formulations for vacancy diffusion and vacancy size. Depending on the material and its microstructure however, these properties may be inaccurate or, because of the difficulty in determining values via experiment, even nonexistent. Such is the case with β-Sn in solder joints and thin films. Much work has been done measuring self-diffusion in bulk Sn via experimental methods using tracer isotopes of $Sn^{113,119,123}$ [5–7], but with few studies examining the finer microstructure and its influence on diffusion [7]. It is in this regime of a material where fast diffusion takes place that is orders of magnitude larger than the pure lattice [8], making quantitative values representing mass transport in the material's microstructure a necessity in modeling failure mechanisms. For a metallic system under electrical load for example, effectively describing the electromigration process at the macroscale requires knowledge of vacancy diffusivity in lattice and grain boundaries, grain coarsening properties, and void flux and formation mechanisms at the microscale, just to name a few.

Knowledge of surface energies for specific orientations of Sn's lattice is a particularly important piece in the characterization of the behavior of solder joints and thin films undergoing electromigration. These energies provide an additional driving force for preferred orientation growth and it has been shown experimentally that β-Sn prefers its (1 0 0) surface when grown on Si(1 1 1) [9]. Surface energies of certain lattice orientations are also a major component in determining the morphology and stability of voids that develop in thin film interconnects under electromigration conditions [10,11]. In addition, diffusion of adatoms on these void surfaces control the overall void flux, with movement highly dependent on anisotropy of diffusivity and direction of the electric current [12].

We can aid in the determination of such transport values, normally computed experimentally, through the use of molecular simulation. Rare-event methods are available specifically for simulating diffusive processes in solid systems—typically slow at simulation timescales—and can be used with relative efficiency on workstation-grade computers or small computing clusters [13–16]. One technique, Henkelman's Dimer method, has been used to calculate activation energies and attempt frequencies of Al adatom diffusive mechanisms with an EAM potential [17]. These compare well to *ab initio* calculations using the Nudged Elastic Band method and require many fewer potential force evaluations, without the knowledge of the initial and final states of the system. In another work, they were able to show preference of multi-atom processes in simulated epitaxial growth of Al and Cu over long timescales [18]. Molecular simulation also aids in the prediction of surface energies. Zhang et al. have used the MEAM potential to successfully calculate

* Corresponding author. Tel.: +1 716 645 1187.
E-mail address: msellers@eng.buffalo.edu (M.S. Sellers).

0169-4332/$ – see front matter © 2010 Elsevier B.V. All rights reserved.
doi:10.1016/j.apsusc.2010.02.038

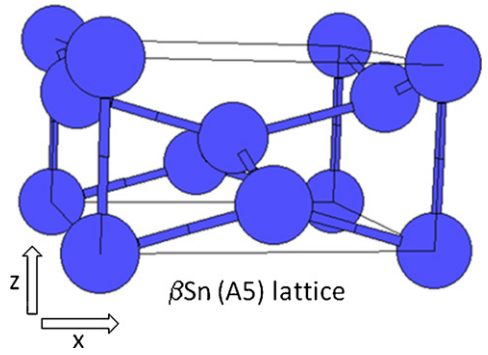

Fig. 1. Shown is the β-Sn (A5) lattice [28]. For the β-Sn phase, the tetragonal lattice constants used are $a = 5.92$ Å and $c = 3.23$ Å. 4 basis atoms are located at (0,0,0), (0.5,0,0.25), (0.5,0.5,0.5), (0.0,0.5,0.75) in lattice coordinates.

surface energies for various FCC and BCC metals, and predicted lowest energy surfaces in agreement with experimental results [19,20]. In the present work, we combine an MEAM potential for Sn and the Dimer method to characterize the surface energies of β-Sn and determine adatom diffusivities for β-Sn's lowest energy surface. To our knowledge, this work is the first study on the calculation of β-Sn surface energies and surface diffusion.

This paper continues with Section 2 explaining in greater detail the calculation of β-Sn surface energies, the Dimer method, and the computation of tracer diffusivities from harmonic transition state theory. We then explain the Simulation details, describing the properties of the simulation cell for surface energy calculation and Dimer method simulations. Finally, Results from the surface energy calculations, dimer simulations, and diffusivity computations are presented and analyzed.

2. Methodology

Below, we present the theory and tools used to calculate surface energies and to conduct the simulations of surface diffusion. LAMMPS software [21,22] is used in conjunction with custom Java code to generate the different Miller plane surfaces of β-Sn and compute their energy relative to a bulk structure. To search for different mechanisms that may occur when an adatom diffuses across a surface, the Dimer method controlled LAMMPS software via custom Java code. For any found mechanisms, we used an approximation to transition state theory and a simple relationship connecting the diffusive prefactor to a mechanism's rate to compute the directional diffusivity of a particular mechanism.

2.1. β-Sn structure

The β-Sn phase, one of the two allotropes of Sn, is metallic and stable at temperatures above 286 K to the melting point of 505 K. It adopts a body-centered-tetratgonal (b.c.t.) structure, shown in Fig. 1, with lattice constants $a = 5.831$ Å and $c = 3.182$ Å. Using the MEAM potential, the equilibrium lattice constants are $a = 5.92$ Å and $c = 3.23$ Å, preserving the 0.546 c/a ratio observed experimentally.

2.2. Interatomic potential

To characterize the atomic interactions of Sn, we use the modified embedded-atom method (MEAM), developed by Baskes. The development of the potential is outlined below and details are given in [23,24].

$$E = \sum_i \left[F_i\left(\frac{\bar{\rho}_i}{Z_i}\right) + \frac{1}{2}\sum_i \phi(r_{ij}) \right] \tag{3}$$

The energy that an atom E_i contributes to the total energy of a system E through interactions with its neighbors is given above. F is the embedding function, or the energy required to embed an atom of type i in to the background electron density ρ_i. This factor is normalized by Z_i, the number of nearest neighbors in the reference structure. The second term, $\phi(r_{ij})$, is the pair interaction between atom i, and its neighbors, j. Sn parameters are listed in Table 1 [25].

These parameters are determined by fitting experimental values of Sn's bulk modulus, average atomic volume, cohesive energy, and equilibrium nearest-neighbor distance of a reference structure of FCC lattice packing. As reported in [20], the potential for Sn has successfully reproduced experimental values of the heat capacity for Sn's α and β phases, as well as the phase transition temperature between liquid and β-Sn, and β- and α-Sn. Details on MEAM's implementation in LAMMPS are available elsewhere [26,27].

2.3. The Dimer method

From a molecular simulation point of view, diffusion in solids is considered a rare event. An atom moving along a surface, in a grain boundary, or through a bulk lattice typically takes many orders of magnitude longer than the timescale of the atomic vibrations, which determines the time step for classical molecular dynamics (MD). Simulations using MD can run for days, or longer, before a significant diffusion event might occur. This inefficiency in direct rare-event simulation has been overcome with methods developed to bridge the two timescales of vibrations and diffusive movement. One popular technique is the Nudged Elastic Band (NEB) method, where once an initial and final state of the system are known, the energy of the path a system can take from state to state is minimized to determine the likely mechanism [13]. Transition Path Sampling (TPS) can also locate likely mechanisms of a state A to state B process by generating an ensemble of dynamical paths from an initial state A to state B path [14]. A third technique developed by Henkelman, called the Dimer method, can locate saddle points on the hyper-surface defined by the model potential energy function, starting only from a minimum energy configuration [16].

While robust in their ability to handle many types of systems, NEB and TPS require the known locations of initial and final states of a system. For this work, we desire a method with the ability to seek out final states and associated saddle points that are perhaps unanticipated. As such, the Dimer method is used in our present study to examine the mechanisms of a diffusing adatom. Henkelman's Dimer method is a potential energy surface walker used to locate saddle point and minimum energy configurations of a system of atoms. It has successfully been used to predict single- and concerted-adatom movement on Cu and Al surfaces and shown to reduce the number of force calculations necessary in saddle point searches, when compared to eigenvector following methods [29]. We apply this method in our surface diffusion study by piecing together parts of a mechanism that a group of atoms might undergo—moving from some *minimum energy state a*, through a *high energy saddle point*, to *minimum energy state b.* A diffusion

Table 1
Parameters for the MEAM potential.

	E_C (eV)	r_0 (A)	a	A	$\beta^{(0)}$	$\beta^{(1)}$	$\beta^{(2)}$	$\beta^{(3)}$	$t^{(1)}$	$t^{(2)}$	$t^{(3)}$	ρ_0
Sn	3.08	3.44	6.20	1.0	6.2	6.0	6.0	6.0	4.5	6.5	−0.183	1.0

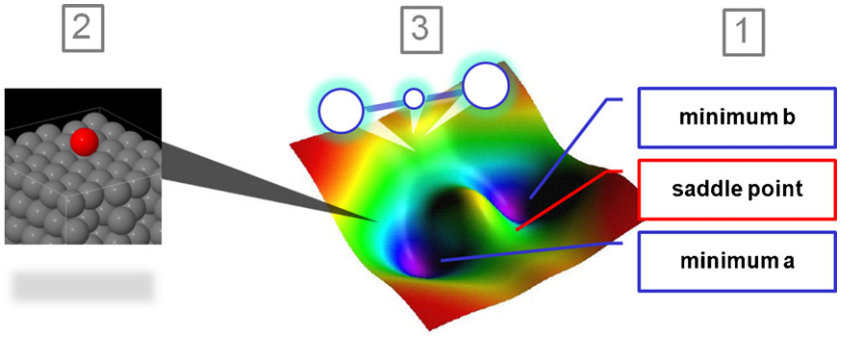

Fig. 2. (1) Typical locations on the energy hyper-surface for minima and saddle points. (2) An atomistic system represented by a point on the energy hyper-surface. (3) Multiple points (systems) with their distance in hyper-surface-space maintained.

mechanism mapped to a potential energy hyper-surface is shown in Fig. 2(1).

Each point on this surface in Fig. 2 represents a specific configuration of atoms. Our system of study, an adatom (red) sitting in a pocket of surface atoms, is shown in Fig. 2(2). We can create two replicas of our system and slightly displace the atoms in each replica, yielding *three* unique points on the hyper-surface, each with different energies and collective atomic positions. With this, a "dimer" on the potential energy hyper-surface is created, shown in Fig. 2(3). If the replica distance in surface-space is maintained, information from the middle and each end of the dimer, such as total energy of each system and the gradient of the energy, provides an estimate for the curvature of the hyper-surface. We can then move the dimer in a direction that leads to a saddle point—a location with one negative mode of curvature and corresponding to a peak in the energy of a diffusion mechanism.

As the dimer is stepped from a low energy region up to a saddle point, it is "'rotated" around its center system in surface-space, to minimize the total energy of the dimer. This ensures that the dimer is following a mode of curvature that leads to a saddle point, and not climbing up some direction of infinitely increasing energy. This minimization is carried out by the steepest descent method. A saddle point is found when the gradient of the energy on the center of the dimer is zero and there is one negative mode of curvature for that system. In this configuration, the dimer can be said to be straddling the saddle point. In Section 3, we present our parameters used in the dimer searches, such as dimer length, number of rotations per step, and saddle point force tolerance.

According to Henkelman, from a saddle point configuration we can find the minimum energy path of a given mechanism using a method similar to the dimer search. We minimize the rotational energy at each step "down" the potential energy surface with a full steepest descent minimization of the rotational energy of the dimer. This is sufficient to keep the dimer on the path of the minimum mode and lessens the number of full force calculations required for minimization. When the energy of the front system of the dimer is greater than the energy of the center system, it has reached a minimum energy configuration (Fig. 3).

2.4. Adatom tracer diffusivity

Once information about the minimum and saddle point for a given mechanism is found, we can use transition state theory (TST) to find its rate constant. For solid systems, the harmonic form of TST is a good approximation to full TST [30], shown below. In this formula ν_i are the vibrational normal mode frequencies at the minimum and saddle point configurations (indicated "init" and "*", respectively), N is the number of atoms, E is the energy of the system at the minimum and saddle configurations, k_B is Boltzmann's constant, and T is temperature.

$$k^{\mathrm{hTST}} = \frac{\Pi_i^{3N} \nu_i^{\mathrm{init}}}{\Pi_i^{3N-1} \nu_i^*} e^{-(E^* - E^{\mathrm{init}})/k_B T} \tag{3'}$$

We can extend hTST to describe the diffusivity of a hopping adatom by computing first, the pre-exponential factor of the Arrhenius form. A review by Gomer [31] provides a relationship for computing this factor, as do and Ratsch and Scheffler [32]. It is shown in Eq. (4). By computing the distance the adatom has traveled from minimum A to minimum B and computing its attempt frequency, shown in Eq. (5), the pre-exponential factor is found.

$$D_0 = \frac{\Gamma l^2}{2\alpha} \tag{4}$$

$$\Gamma = \frac{\Pi_i^{3N} \nu_i^{\mathrm{init}}}{\Pi_i^{3N-1} \nu_i^*} \tag{5}$$

Here, Γ is the attempt frequency and ν_i are the normal modes at the minimum (init) and saddle point (*) for an N atom system, l is the distance traveled by the adatom, and α is the dimensionality of the lattice ($\alpha = 2$ for a square lattice, 1 for a specific diffusion direction x or y or z). From our dimer searches, we can find E_A, the difference in energies of the saddle and minimum configurations, and using the relation for D_0, we can compute the diffusivity, D^* for a particular mechanism, expecting a simple Arrhenius relationship, as in Eq. (7).

$$D^* = D_0 e^{-E_A/kT} \tag{6}$$

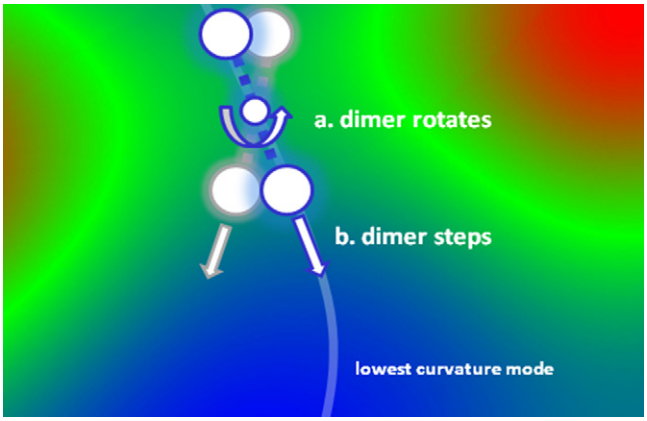

Fig. 3. When tracing the path of minimum energy from the saddle point to minimum, the dimer is rotated to a minimum energy via steepest descent (a) and then stepped (b), maintaining the correct orientation along the lowest curvature mode. This routine is repeated until the center of the dimer is at a minimum energy.

Table 2
Dimer method parameters.

	Length (Å)	Step length (Å)	Step converg.	Rot. converg.	Rot./step
Saddle	0.001	0.025	$F_{center} < 0.1$ eV/Å	$F_{rot} < 0.1$ eV/Å	2 max
Min	0.003	0.001	$E_{front} > E_{center}$	$F_{rot} < 0.1$ eV/Å	Until converg.

3. Simulation details

In creating the surfaces for our surface energy calculation, the solid lattice was rotated so its surface normal vector was perpendicular to the *z*-axis of the simulation cell. The system was periodic in the *x* and *y* axes and the *z* height fixed. This allowed for the creation of a two-surface slab. The thickness of the slabs was such that the two surfaces did not interact with one another. Typically, this is a value greater than twice the potential cutoff—ours often surpassed this and was dependent on the spacing between periodic Miller planes in the simulation cell *z*-direction. We use Eq. (7) to compute the surface energy relative to the bulk. A mathematically equivalent form is used by Zhang et al. [19,20].

$$\gamma_s = \frac{E_{slab} - (E_{coh} \cdot N_{atoms})}{2 \cdot A} \quad (7)$$

In Eq. (7), γ_s is the excess surface energy when compared to a bulk structure. E_{slab} is the energy of the system containing two surfaces, periodic in *x* and *y*. E_{coh}, the bulk cohesive energy (energy per atom), is multiplied by N_{atoms}, the number of atoms in our slab system. The numerator is divided by 2 to account for two surfaces, and is scaled by the area *A* of one surface.

While the static (0 K) system and relationship in Eq. (7) offer a straightforward way to compute excess surface energies from molecular simulation, one might consider other choices for the quantitative comparison of unlike material surfaces. To unite the many relations and perceived inconsistencies in units of surface energy, Zhao et al. proposed the extension of the bond-order-length-strength (BOLS) correlation that quantifies a volume-based energy density and incorporates the effect of temperature [33]. Key components here are the representation of atomic bond contraction of under-coordinated surface and near-surface atoms, thermal expansion of the lattice, and their resulting effect on bond strength. For a more detailed investigation of surface energetics, the work of Zhao et al. may be considered.

For our dimer simulations, the simulation cell consisted of a 4*x*–4*y*–6*z* block of β-Sn lattice with a single Sn adatom on the (1 0 0) surface. This surface is parallel to the *YZ* plane and the cell is periodic in these directions. A total of 217 atoms made up the system, governed by the MEAM potential with a cutoff of 4.5 Å. Initially, an adatom was placed at random on the (1 0 0) surface and allowed to equilibrate to a low energy configuration using molecular dynamics. We presumed (and confirmed visually) that the adatom was now seated in a low energy pocket on the (1 0 0) surface. From this initial configuration, the dimer searches were carried out. Atoms within a distance of 8.7 Å of the adatom are allowed to move, shown in Fig. 4. Before starting the search, the movable atoms close to the adatom were all displaced by a value between −0.2 and 0.2 Å, drawn from a Gaussian distribution, increasing the dimer's ability to locate different low lying saddle point configurations. Once a saddle point configuration was found, the dimer was marched back along the lowest curvature mode to verify that it ended up in the initial minimum region. In Table 2 are the parameters used in the dimer saddle point and minimum searches. The energy of the saddle point, minimum region, and periodic points along the minimum energy path (lowest curvature mode) were saved. All atoms in the simulation are included in determining the specific energy of a configuration.

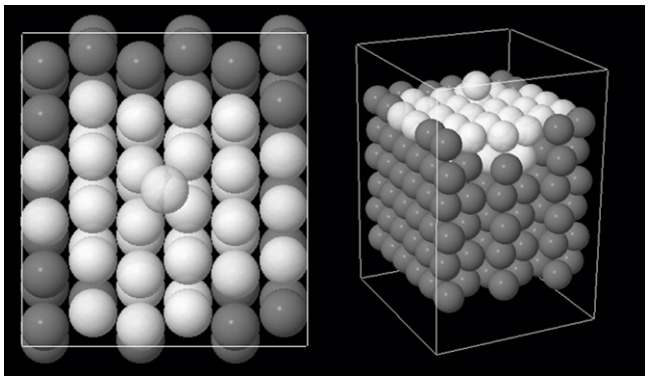

Fig. 4. (Left) A *z*-direction, top view of the (1 0 0) surface. (Right) A three-dimensional view of the simulation cell. Atoms are colored white to denote movable by the Dimer method and gray for fixed.

At saddle point and minimum energy configurations only the 37 movable atoms are included in the vibrational normal mode frequency calculations. We computed the vibrational normal modes assuming atoms behaved as harmonic oscillators and developed a $3N \times 3N$ matrix of the gradient of the force. The eigenvalues of this matrix are the normal modes of the system and were converted to vibrational frequencies.

4. Results and discussion

4.1. Surface energy calculation for b.c.t. β-Sn

We calculated excess surface energies of the (1 0 0), (1 1 0), (1 0 1), (1 1 1), (2 1 0), and (2 0 1) un-relaxed surfaces for β-Sn using the relation shown in Eq. (7) and a simulation setup described in Section 3. Results from these calculations are shown in Table 3, along with results from FCC surface energy calculations for Cu, Ag, and Al from Zhang et al. [19]. It is straightforward to identify the lowest energy surface for each of these elements—for Cu, Ag, and Al in an FCC crystal structure the lowest energy surface is (1 1 1), while for β-Sn our calculations show that (1 0 0) is the lowest energy surface. For cubic structures, the (1 0 1) surface is equivalent to the (1 1 0) surface, as is (2 1 0) and (2 0 1).

4.2. Surface diffusion on (1 0 0)

Dimer searches were conducted starting from a low energy configuration of our adatom (1 0 0) surface system, equilibrated via low temperature molecular dynamics. The dimer searches provide

Table 3
Surface energies γ_s of β-Sn, Cu, Ag, and Al with respect to Miller plane orientation. Cu, Ag, and Al are reproduced from [19].

hkl	γ_s (eV/A^2)			
	β-Sn	Cu	Ag	Al
1 0 0	0.0497	0.1030	0.0795	0.0561
1 1 0	0.0622	0.1024	0.0765	0.0606
1 0 1	0.0569	–	–	–
1 1 1	0.0646	0.0879	0.0681	0.0386
2 1 0	0.0671	0.1069	0.0792	0.0666
2 0 1	0.0684	–	–	–

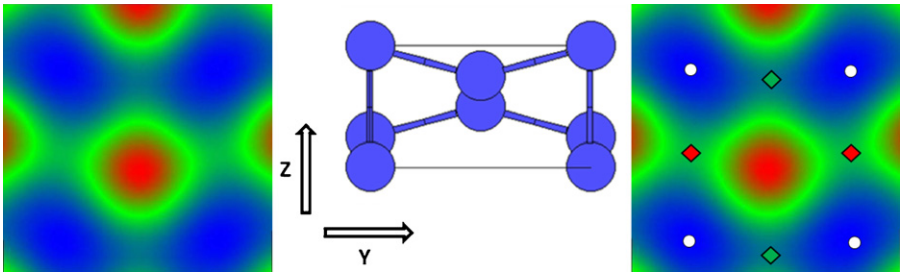

Fig. 5. Energy maps of the β-Sn (1 0 0) surface. (Left) Red denotes a higher energy (ion cores), blue denotes lower energy. (Right) Diamonds are respective saddle point locations of the adatom, white circles are minima locations.

Table 4
Mechanism data. Respectively, the adatom direction, mechanism activation energy, attempt frequency, distance the adatom traveled, and tracer diffusivity at 300 K are specified.

Mechanism	E_A (eV)	Γ (THz)	l (Å)	D ($\times 10^{-06}$ cm^2/s) 300 K
c-Direction	0.1493	1.17	3.23	1.893
a-Direction	0.1138	0.745	2.96	3.994

information about the saddle point and minimum configurations for a given mechanism, and with this data we computed the theoretical tracer diffusivity for each mechanism found.

In our system a large number of configurational degrees of freedom exist, and we rely on the Dimer method to seek out and find the many possible low lying saddle points available to the system as it undergoes some diffusive transition. More than 1000 searches, starting with random orientations of the dimer, converged to only three types of mechanisms. The first two involved the adatom moving across the surface in a hop mechanism. The third was a variety of different movements of the surface atoms, where atoms far removed from the adatom would "pop-up" out of the surface slightly. These would lead the system to a saddle point, as well as back to the initial minimum, but a second minimum was simply a partially raised surface atom and no movement of the adatom. Therefore, we considered only mechanisms in which the adatom moved. With this restriction, we found only the two hopping mechanisms contribute to adatom movement.

It is fairly straightforward to enumerate the saddle points a diffusing adatom would encounter hopping across the (1 0 0) face of a β-Sn lattice. Fig. 5 illustrates the (1 0 0) surface of β-Sn in an energy map, created by rasterizing the surface with an atom at a distance of 2.0 Å above and recording the energy. The high energy ion core locations are shown in red, while the low energy pockets are shown in blue. Referring to this figure, it is quite clear where the saddle point for a single atom diffusion transition might be located. We have labeled the energy map with the location of the common minimum and two unique saddle points found in our Dimer method searches and minimum energy path traces.

The two mechanisms found were a relatively simple movement of the adatom from one minimum energy pocket to the next closest minimum energy pocket. Looking at the (1 0 0) plane in Fig. 5, these translate to a *z*-direction movement (lattice *c*-direction) of the adatom and a *y*-direction movement (lattice *a-direction*) of the adatom. If a system started at one of the specified minimum configurations (white circles in Fig. 5), it could either move in the positive or negative *c*-direction through a saddle point (indicated by the red diamond) or in the positive or negative *a-direction* (indicated with a green diamond). Specific data from these mechanisms is shown in Table 3 and the energy values along the minimum energy path are shown in Fig. 6 as red and green curves.

With the results of the dimer search, vibrational analysis, and displacement measurements, we computed the theoretical tracer diffusivity of the adatom for each mechanism at a temperature of 300 K using Eqs. (5)–(7). The factor α for these diffusivities is taken to be 1 because the mechanisms move the adatom in only one dimension. Shown in Table 4 are our values for attempt frequency, activation energy, and diffusivity at 300 K.

Ratsch and Scheffler [32] report that for Ag adatom on an Ag (1 1 1) surface, as the number of degrees of freedom considered in the vibrational normal mode frequency calculation increase, the attempt frequency decreases. For their largest normal mode frequency calculation, they compute an attempt frequency value of

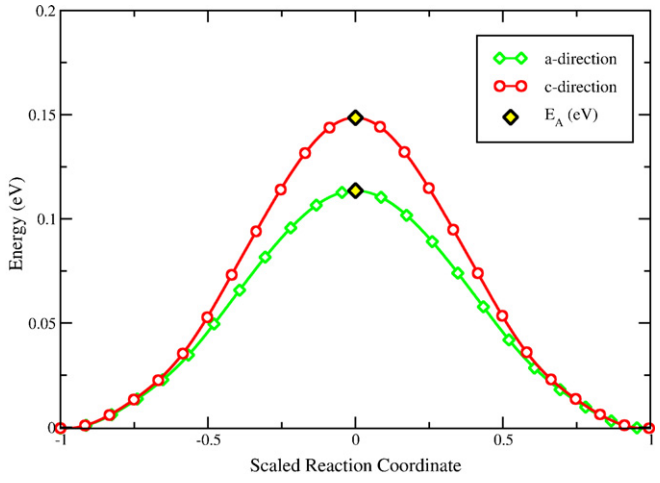

Fig. 6. Energy values along the minimum energy path for the given mechanisms. Values along the reaction coordinate are corrected to a baseline value of the minimum energy configuration—both mechanisms begin and finish at 0 eV. Diamonds denote energies corresponding to saddle point configurations.

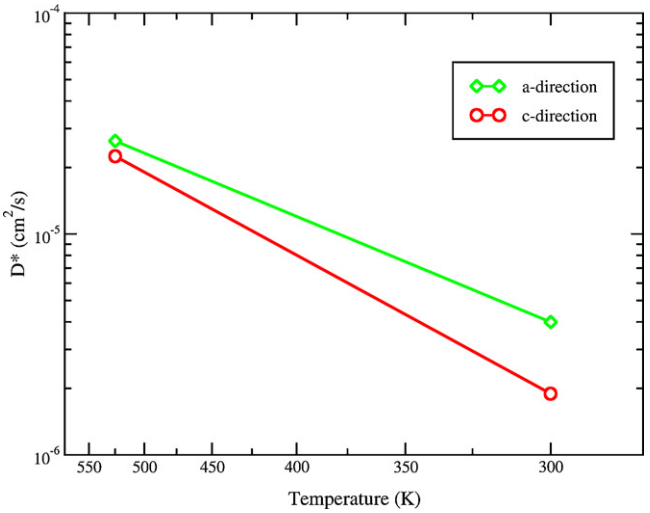

Fig. 7. Arrhenius plot of diffusivity with respect to temperature.

0.71 THz, where $3N = 99$ and N is the number of atoms included. This result is similar to our calculations shown in Table 4. In addition, their activation energy was calculated at 0.082 eV for an adatom hopping on the (1 1 1) surface of Ag, known to be FCC's lowest energy surface, and compares on a similar scale to our measurements for an adatom hoping on β-Sn's lowest energy surface. In contrast, Henkelman's results for Cu and Al adatom activation energies on higher energy (1 0 0) surfaces are 2–3 times larger than our values [17,18].

Additional values of the theoretical tracer diffusivity for each mechanism are computed via the previously mentioned relations and an Arrhenius plot of diffusivity vs. temperature is shown in Fig. 7. The y-axis is in logarithmic scale and the x-axis is in inverse temperature scale. Here, β-Sn's lattice anisotropy clearly plays a role in the directional diffusivity. At high temperatures however, this difference is less pronounced.

5. Conclusions

Our calculations of surface energies of various low index Miller planes of the β-Sn phase indicate that the (1 0 0) surface has the lowest excess surface energy. A preference for the (1 0 0) surface has been shown in experiment, and our results using the MEAM potential confirm that from a surface energy minimization standpoint, the (1 0 0) surface preference should be exhibited in most epitaxial growth experiments. In addition, we also provide a list of surface energies for use in studies of void migration in β-Sn. We have also shown results for the diffusivity of a Sn adatom on a β-Sn (1 0 0) surface via theoretical and numerical methods. The adatom on the (1 0 0) surface exhibited hopping diffusion mechanisms in the *a*-direction and *c*-direction of the lattice. Attempt frequencies and activation energies were slightly different for each type of system. The differences in each case correspond to unique behaviors of diffusivity with respect to temperature and directionality of diffusion.

In all our dimer simulations, we did not observe any concerted atom rearrangement like that of the Cu and Al (1 0 0) surfaces that Henkelman simulated. We believe this is most likely due to the apparent layering of the β-Sn lattice in the [1 0 0] direction. An FCC lattice exhibits a tight, alternating packing in the [1 0 0] direction for successive (2 0 0) lattice planes, providing a physically and energetically deeper pocket for an adatom to sit on its surface, evidenced in Table 3. This may cause mechanisms involving concerted rearrangements to have activation energies similar to those involving adatom hopping. While for β-Sn, successive (2 0 0) surfaces in the [1 0 0] direction appear shifted with respect to FCC. Atoms in the faces of β-Sn's b.c.t. structure fall closer in line with its corner atoms along the [1 0 0] direction, creating sheet-like layers of atoms. Accordingly, an adatom on the energetically smoother (1 0 0) layer of β-Sn may move much more freely by hopping than taking part in surface atom rearrangement.

Acknowledgements

This work is supported by the National Science Foundation, grants CMMI-0508854 and CHE-0626305, and the Office of Naval Research Advanced Electrical Power Systems Division. Calculations were performed using resources from the University at Buffalo Center for Computational Research.

References

[1] R. Kirchheim, Materials Research Society Symposium Proceedings 309 (1993) 101–110.
[2] R. Kirchheim, Acta Metallurgica et Materialia 40 (2) (1992) 309–323.
[3] C. Basaran, M. Lin, H. Ye, International Journal of Solids and Structures 40 (26) (2003) 7315–7327.
[4] C. Basaran, M. Lin, International Journal of Materials and Structural Integrity 1 (1,2,3) (2007) 16–39.
[5] F.H. Huang, H.B. Huntington, Physical Review B 9 (4) (1974) 1479–1487.
[6] P.H. Sun, M. Ohring, Journal of Applied Physics 47 (2) (1976) 478–485 (and references therein).
[7] P. Singh, M. Ohring, Journal of Applied Physics 56 (3) (1984) 899–907.
[8] R. Kirchheim, U. Kaeber, Journal of Applied Physics 70 (1991) 172–181.
[9] J.T. Ryu, T. Fujino, M. Katayama, Y.B. Kim, K. Oura, Applied Surface Science 190 (2002) 139–143.
[10] D. Kim, W. Lu, Journal of the Mechanics and Physics of Solids 54 (2006) 2554–2568.
[11] W. Wang, Z. Suo, Journal of Applied Physics 79 (5) (1996) 2394–2403.
[12] M. Gungor, D. Maroudas, Journal of Applied Physics 85 (4) (1999) 2233–2246.
[13] H. Jónsson, G. Mills, K. W. Jacobsen, Nudged Elastic Band Method for Finding Minimum Energy Paths of Transitions, Classical and Quantum Dynamics in Condensed Phase Simulations', in: B. J. Berne, G. Ciccotti, D. F. Coker (eds.) (World Scientific, 1998) 385.
[14] P.G. Bolhuis, D. Chandler, C. Dellago, P.L. Geissler, Annual Reviews in Physical Chemistry 53 (2002) 291–318.
[15] M.R. Sorensen, Y. Mishin, A.F. Voter, Physical Review B 62 (6) (2000) 3658–3672.
[16] G. Henkelman, H. Jonsson, Journal of Chemical Physics 111 (15) (1999) 7010–7022.
[17] G. Henkelman, H. Jonsson, Journal of Chemical Physics 115 (21) (2001) 9657–9665.
[18] G. Henkelman, H. Jonsson, Physical Review Letters 90 (11) (2003) 116101/1–116101/4.
[19] J.-M. Zhang, F. Ma, K.-W. Xu, Applied Surface Science 229 (2004) 34–42.
[20] J.-M. Zhang, D.-D. Wang, K.-W. Xu, Applied Surface Science 252 (2006) 8217–8222.
[21] LAMMPS Simulator, http://lammps.sandia.gov (2009).
[22] S.J. Plimpton, Journal of Computational Physics 117 (1995) 1–19.
[23] M.I. Baskes, Physical Review B 46 (5) (1992) 2727–2742.
[24] M.I. Baskes, Modeling Simulation in Materials Science Engineering 2 (1994) 505–518.
[25] R. Ravelo, M.I. Baskes, Physical Review Letters 79 (13) (1997) 2482–2485.
[26] H. Huang, N. Ghoniem, J. Wong, M.I. Baskes, Modeling Simulation in Materials Science Engineering 3 (1995) 615–627.
[27] Gullet, G.M., Wagner, G., Slepoy, A., Sandia Report SAND2003-8782.
[28] NRL Crystal Lattice, http://cst-www.nrl.navy.mil/lattice/ (2009).
[29] R.A. Olsen, G.J. Kroes, G. Henkelman, A. Arnaldsson, H. Jonsson, Journal of Chemical Physics 121 (20) (2004) 9776–9792.
[30] C. Wert, C. Zener, Physical Review 76 (8) (1949) 1169–1175.
[31] R. Gomer, Reports on Progress in Physics 53 (7) (1990) 917–1002.
[32] C. Ratsch, M. Scheffler, Physical Review B 58 (19) (1998) 163–166.
[33] M. Zhao, W. Zheng, L. Jianchen, Z. Wen, Physical Review B 75 (8) (2007).